EUROPEAN JOURNAL OF REMOTE SENSING
2023, VOL. 56, NO. 1, 2231137
https://doi.org/10.1080/22797254.2023.2231137

Prediction of land use and land cover change in two watersheds in the Senegal River basin (West Africa) using the Multilayer Perceptron and Markov chain model

Mame Henriette Astou Sambou[a,b], Jean Albergel[b], Expédit Wilfrid Vissin[c], Stefan Liersch[d], Hagen Koch[d], Zoltan Szantoi[e,f], Wassim Baba[f], Moussé Landing Sane[g] and Ibrahima Toure[g]

[a]Climate Change and Water Resources, West African Science Service Centre on Climate Change and Adapted Land Use (WASCAL), Université d'Abomey-Calavi, Cotonou, Benin; [b]Montpellier SupAgro, IRD, University of Montpellier, Montpellier, France; [c]Laboratoire Pierre PAGNEY, Climat, Eau, Ecosystème Et Développement (LACEEDE), Université d'Abomey-Calavi (République du Bénin), Abomey Calavi, Benin; [d]Climate Resilience, Hydroclimatic Risks, Potsdam Institute for Climate Impact Research (PIK), Postdam, Germany; [e]Laboratoire Pierre PAGNEY, Climat, Eau, Ecosystème et Développement (LACEEDE), Stellenbosch University, Abomey Calavi, Benin; [f]Science, Applications & Climate Department, European Space Agency, Frascati, Italy; [g]Faculty of Sciences and Technology, Department of Physics, Cheikh Anta Diop University, Dakar, Senegal

ABSTRACT

Land use and Land cover change (LULCC) is a major global problem, and projecting change is critical for policy decision-making. Understanding LULCCs at the watershed level is essential for transboundary river basin management. The present study aims to analyse the past and future LULCCs in two significant watersheds of the Senegal River basin (SRB) in West Africa: Bafing and Faleme. This study used Landsat images from 1986, 2006 and 2020 and the Random Forest classification method to analyze past LULCCs in these two watersheds. The results revealed: In Bafing, vegetation, settlement, agricultural areas and water increased, while the bareground decreased significantly between 1986-2020. In Faleme, two periods have different trends. Between 1986-2006, vegetation, settlement, agricultural areas and water increased, while bareground decreased. Between 2006-2020, settlement increased, while vegetation, agricultural areas, water and bareground decreased. To predict LULCCs in 2050 under business-as-usual assumptions, the Multilayer Perceptron and Marcov Chain model (MLP-MC) was used. The MLP-MC shows better results on Bafing than on Faleme but without questioning its application on the two watersheds. Bafing has seen a trend towards "more people, more trees", while Faleme has seen a trend towards "more people, more deforestation". These results contribute to develop appropriate land management policies and strategies to achieve or to maintain sustainable development in the SRB.

ARTICLE HISTORY
Received 21 January 2023
Revised 16 June 2023
Accepted 26 June 2023

KEYWORDS
Land use land cover change; multi-temporal analysis; MLP-MC; Random forest; Senegal river basin

Introduction

Land use and land cover change (LULC) is a challenge and a key focus of global change research. Land use (habitat, agricultural) and land cover (forests, wetlands, grasslands and water) have different meanings and are often used interchangeably (Tadese et al., 2021). LULC changes are the result of changes in the Earth's land surface, such as the transformation of natural land cover (forests, grasslands and deserts) into human-dominated ecosystems (cities, agricultural and industrial areas) (Liping et al., 2018; Winkler et al., 2019). These changes significantly affect critical elements of our natural capital, such as vegetation, water resources and biodiversity (Chang et al., 2018; Solly et al., 2021). The dynamics of LULC change are not the same in all regions of the world due to different driving factors (Berihun et al., 2019). Although anthropogenic factors have been proven to be the main drivers of changes, factors such as climate, slope, appearance and altitude can also influence these changes (Anwar et al., 2022; Mekonnen & Manderso, 2023). In West Africa (WA), notable LULC changes have been observed (Andrieu, 2018; Barnieh et al., 2020; Cabral & Lagos, 2017; Diallo & Zhengyu, 2018; A. Traore et al., 2018; S. S. Traore et al., 2022). These authors shown that WA has undergone significant changes over the years, and the causes are generally attributed to rapid population growth and increased agricultural areas. Even if the information on LULC changes at the regional or national scale is available, it is essential to study at the local scale (Fikadu & Olika, 2023). Indeed, studies of watershed-based LULC changes are crucial tools for policymakers, planners and local communities to formulate appropriate policies and strategies in the future (Berihun et al., 2019; Thiam et al., 2022).

Advances in remote sensing and Geospatial Information Systems (GIS) have resulted in high-resolution products and LULC models for mapping,

CONTACT Mame Henriette Astou Sambou astmyma@yahoo.fr Dakar, Senegal

detecting and predicting LULC changes (Liping et al., 2018; S. K. Singh et al., 2015; Wang et al., 2021). Google Earth Engine (GEE) is an open-source, cloud-based geospatial processing platform that provides free access and open-source satellite datasets (Landsat, Modis, Sentinel) with a high spatial resolution for extended periods (L. Yang et al., 2022). Google Earth Engine (GEE) is the most popular big geo data processing platform, which provides a set of state-of-the-art classifiers for pixel-based classification used for LULC mapping. The main advantage of GEE is the close link between the data and the algorithms, both of which are accessible via an Application Programming Interface (API) (Gorelick et al., 2017; Shelestov et al., 2017). Due to its accessible and user-friendly design, it has grown in popularity recently (Dubertret et al., 2022; Jampani et al., 2020; Nasiri et al., 2022; Ougahi & Mahmood, 2022).

The success of any LULC mapping depends on several factors, including the choice of an appropriate classification algorithm (Lu & Weng, 2007). Advanced classification algorithms such as Regression Trees (CART), Random Forest (RF), kNearest Neighbor (k-NN), Support Vector Machine (SVM), Artificial Neural Network (ANN), Multinomial Logistic Regression (MLR), Maximum Likelihood Classification (MLC), and Bayesian classifiers have attracted considerable attention in image classification for LULC mapping (Ma et al., 2019; Macarringue et al., 2022). Authors such as A. D. Kulkarni and Lowe (2016) and Talukdar et al. (2020) have conducted comparative studies between several classification algorithms to identify the most suitable and accurate classification algorithm for LULC mapping. Their results indicated that Random Forest showed the best performance for the LULC classification compared to other classifiers. The main factors behind its widespread use in multitemporal LULC classification are (1) effective management of outliers and noisy datasets; (2) satisfactory results with multi-source and high-dimensional datasets; (3) superior accuracy to other widely used classifiers, like SVM or MLC in many applications; and (4) speeding up processing by concentrating on essential factors (Amini et al., 2022; Noi Phan et al., 2020).

Modelling LULC changes using remote sensing data and determining factors helps answer the question of how LULC change and how it may change in the future (Sankarrao et al., 2021). Several methods have been adopted to predict future LULC changes. These methods can be classified into non-hybrid and hybrid methods. The non-hybrid approaches, such as Markov Chain (MC), Artificial Neural Network (ANN), Cellular Automata (CA), have been widely used to identify the transitions in LULC classes and have been accurate in predicting LULC changes (Silva et al., 2020; V. G. Singh et al., 2022). The Non-hybrid methods have limitations in predicting LULC changes (Noszczyk, 2019). To overcome the limits of individual models, hybrid models have been introduced by combining several modelling approaches to address the complexity of real-world systems (Gaur et al., 2020). The hybrid models can capture LULC changes with greater accuracy (Gaur et al., 2020; Sankarrao et al., 2021). Clark Labs developed an integrated LULC model based on GIS and remote sensing, known as the Land Change Modeler (LCM), to explore future changes in LULC using a Multilayer Perceptron neural network (MLP) and Markov chain (MC) (V. Mishra et al., 2014). Given its robustness and popularity, the MLP-MC model seems the most suitable for modelling spatiotemporal dynamics and projecting future LULC change scenarios. Gaur et al. (2020) used hybrid and non-hybrid models to capture LULC scenarios for the Subarnarekha River and found that the MLP_MC model was the best-suited model. Examples of applications can be found in (Fathizad et al., 2015; Leta et al., 2021; V. N. Mishra et al., 2018; Sankarrao et al., 2021).

The Upper Senegal River Basin (SRB), located in WA, is a transboundary basin bordered by four countries: Guinea, Mali, Mauritania and Senegal. It is formed by several watersheds. Understanding LULC changes at a watershed level in transboundary watershed management is crucial (Thiam et al., 2022). Unfortunately, there are few studies on LULC changes in the SRB. Only one previous study was conducted by Faty (2017). Faty (2017) used Modis-Terra satellite data from 2007 and 2014 and maximum likelihood classification to analyze the LULC dynamics across the SRB. The main limitation of this study is that the author evaluated the LULC changes considering that all watersheds constitute a single socioeconomic, land and agricultural environment. The author didn't consider the influence of the socioeconomic configuration specific to each watershed. Although LULC change is a common phenomenon, it is challenging to generalize trends within a particular region, such as the SRB (Berihun et al., 2019). In addition, no study has attempted to simulate the future trends of LULC changes considering each watershed in the SRB. Therefore, as part of this study, we aim to fill these knowledge gaps to understand the spatiotemporal variability of LULC changes in two watersheds in different socioeconomic and agricultural environments at the SRB: the Bafing and the Faleme. This study aims: (i) to map the LULC (1986, 2006 and 2020) in the two sub-watersheds with the Random Forest (RF) classification method; (ii) to simulate the future trends of LULC change of 2050 based on the hybrid model (MLP_MC) in LCM and (iii) to analyze the spatiotemporal variability of LULC in these two watersheds. This study is relevant for the riparian states of the Senegal River basin grouped into the organization for the

development of the Senegal River (OMVS) to evolve policies specific to each watershed.

Materials and methods

Study area

The study area is in the SRB, between Senegal, Mali, Mauritania and Guinea Conakry (Figure 1). The two watersheds belong to different administrative regions:

- The Bafing is the main constituent of the Senegal River and originates near Mamou (Guinea Conakry) (nearly 1,000 m above sea level). It extends between latitudes 10°30“and 12°30” N and longitudes 12°30’ and 9°30‘W and covers northwest Guinea Conakry and southeastern Mali. It drains the entire eastern part of the Fouta Djalon and feeds the Manantali Hydropower dam (Sambou et al., 2023)
- The Faleme also has its source in the northern foothills of the Fouta Djalon in Guinea Conakry. It is a major tributary of the Senegal River, which it joins at the meeting point of the borders of Senegal and Mali at the level of the city of Ballou. The Faleme lies between latitudes 12° 11′–14°27′N and longitudes 11° 12‘–12°15‘W in the humid tropical regions and the southern margins of the Sahel. The main biophysical

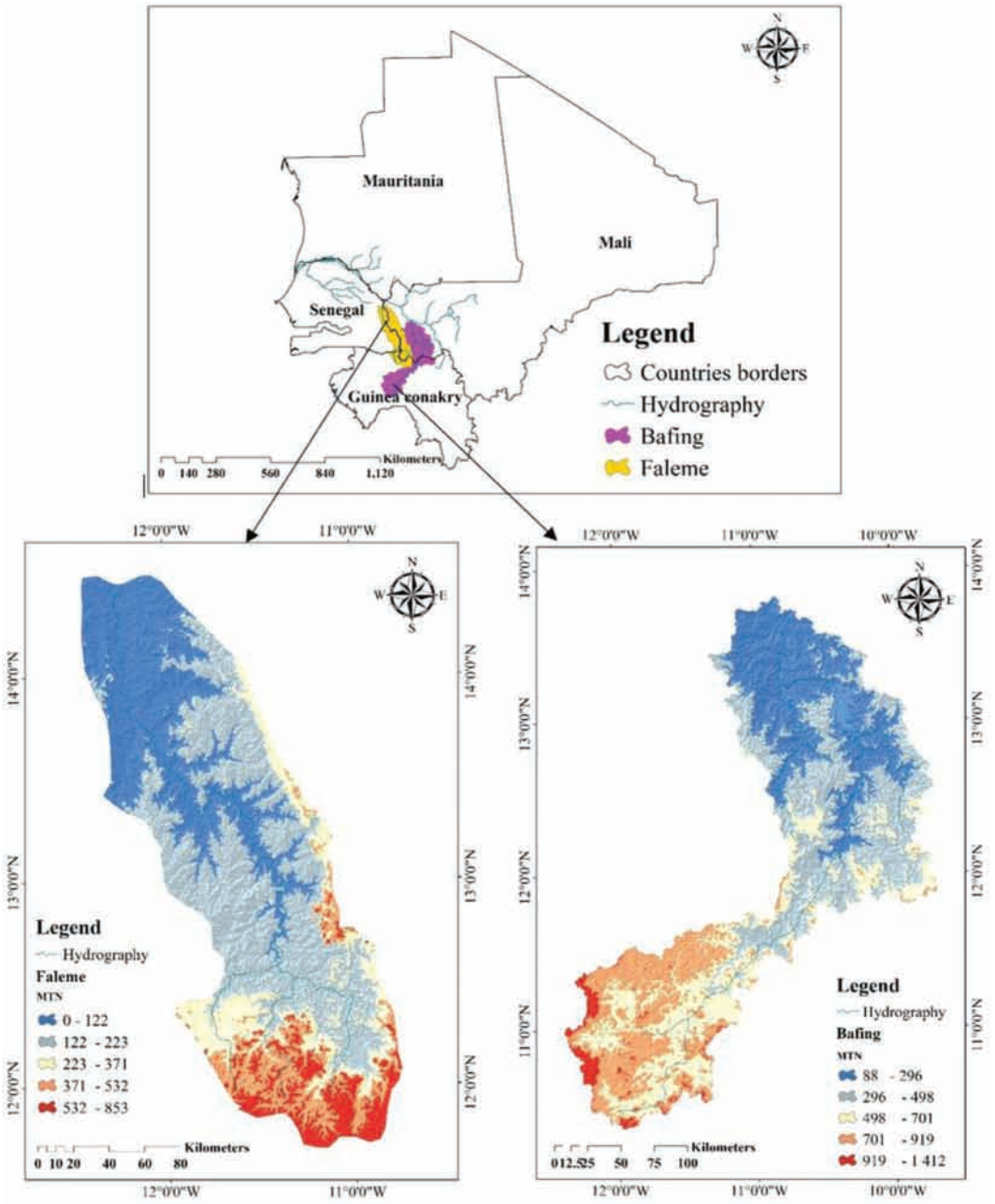

Figure 1. Location map of the bafing and faleme in the SRB in WA, between senegal, mali, Mauritania, and guinea conakry.

characteristics of the watersheds studied in the SRB are presented in Table 1.

Data source

The acquisition of satellite images is the first step in LULC mapping. The choice of satellite images is based on four criteria: spatial coverage, spatial resolution, available years, and cloudiness (minimum) (Horning, 2004; Martignac,). Landsat satellite images were chosen, in this study. It is the oldest of the earth observation programs, thus having an archive of images over a long period (more than 30 years) (Woodcock et al., 2008). It offers a sufficient level of detail to identify the characteristics of the LULC. Google Earth Engine (GEE) provides surface reflectance images that are corrected atmospherically and improve the detection of changes (Wahap & Shafri, 2020). The images selected are presented in Table 2. As supplementary input data, we included the digital elevation model (DEM) (ALOS World 3D–30 m), distance from the road, distance from the river, and distance from the settlement.

Land use and land cover mapping

This study used GEE (Gorelick et al., 2017; Shelestov et al., 2017) to build the LULC map through Landsat image processing, supervised classification, and classification accuracy. Figure 2 describes the general steps followed to make the maps. Details will be provided in the following sections.

Preprocessing

Orthorectified and atmospheric corrected Landsat Surface Reflectance Tier 1 images available for Landsat OLI/TIRS and MSS/TM sensors were collected in GEE for the years of interest (1986,2006,2020). The cloud cover function in GEE was applied to select the collection of annual images with a cloud cover of < 15%. The median ee.Reducer function on GEE was then used to "reduce" the image collection to a single output image representing the median of the images (Dubertret et al., 2022; Noi Phan et al., 2020).

Construction of features

The spectral and topographic features were combined as input features for LULC classification algorithm. For spectral characteristics, blue, green, red, Near Infrared (NIR), and Shortwave Infrared (SWIR) spectral image bands were selected because they have the potential to discriminate similar spatiotemporal phenomena, thus improving the separability of LULC classes (Thiam et al., 2022). In addition, numerous studies have shown that the use of spectral features from indices such as normalized difference vegetation index (NDVI) (1), normalized water difference index (MNDWI) (2), normalized difference accumulation index (NDBI) (3) as input features for classification will effectively improve the accuracy of LULC (K. Kulkarni & Vijaya, 2021; Tsai et al., 2018). Indeed, the NDVI supplies information on the characteristics of the vegetation cover. The NDWI provides information on the characteristics of water bodies. The NDBI is used to get the artificial characteristics of the earth's surface. In addition, topographical features such as altitudes and slopes increase the accuracy of land cover classification (Y. Yang et al., 2021). Hence, the elevation and slope data were extracted from the DEM as features for LULC classification (Table 3).

$$\mathrm{NDVI} = \frac{\mathrm{NIR} - \mathrm{Red}}{\mathrm{NIR} + \mathrm{Red}} \tag{1}$$

$$\mathrm{MNDWI} = \frac{\mathrm{Green} - \mathrm{SWIR}}{\mathrm{Green} + \mathrm{SWIR}} \tag{2}$$

$$\mathrm{NDBI} = \frac{\mathrm{SWIR} - \mathrm{NIR}}{\mathrm{SWIR} + \mathrm{NIR}} \tag{3}$$

Classification

In this study, the RF classification algorithm was used to produce LULC maps for years 1986, 2006,

Table 1. The main biophysical characteristics of the watersheds. Source: (Sane et al., 2020).

Characteristics	Bafing	Faleme
Area (Km2)	39.01	28.05
Mean Annual Temperature (C)	28.3	29.3°C
Agro-Ecology Zone	Guinean Sudano	Guinean Sudano
Mean Annual Rainfall (mm)	1166	800
Major Soil Type	Gres Qtz., Dolerites, Granite, Sandstone	Shale, Gres Qtz., Dolerites, Granites
Dominant Crop	Cassava, Maize, Fonio, Sorghum and Millet.	Maize, Rice, Millet, and Sorghum.
Dominant Livestock	Bovine	Bovine
Activities	Fishing, Agriculture area, Livestock, Bauxite Mining	Fishing, Agriculture area, Livestock, Gold Mining

Table 2. Characteristics of Landsat images selected for the LULC mapping.

Dataset	Satellite	Sensor	Spatial resolution	Date of acquisition	Band
Image 1	USGS Landsat 5 (Surface Reflectance Tier 1)	MSS/TM	30 m	1986	Multispectral
Image 2	USGS Landsat 5 (Surface Reflectance Tier 1)	MSS/TM (Surface Reflectance Tier 1)	30 m	2006	Multispectral
Image 3	USGS Landsat 8 (Surface Reflectance Tier 1)	OLI/TIRS (Surface Reflectance Tier 1)	30 m	2020	Multispectral

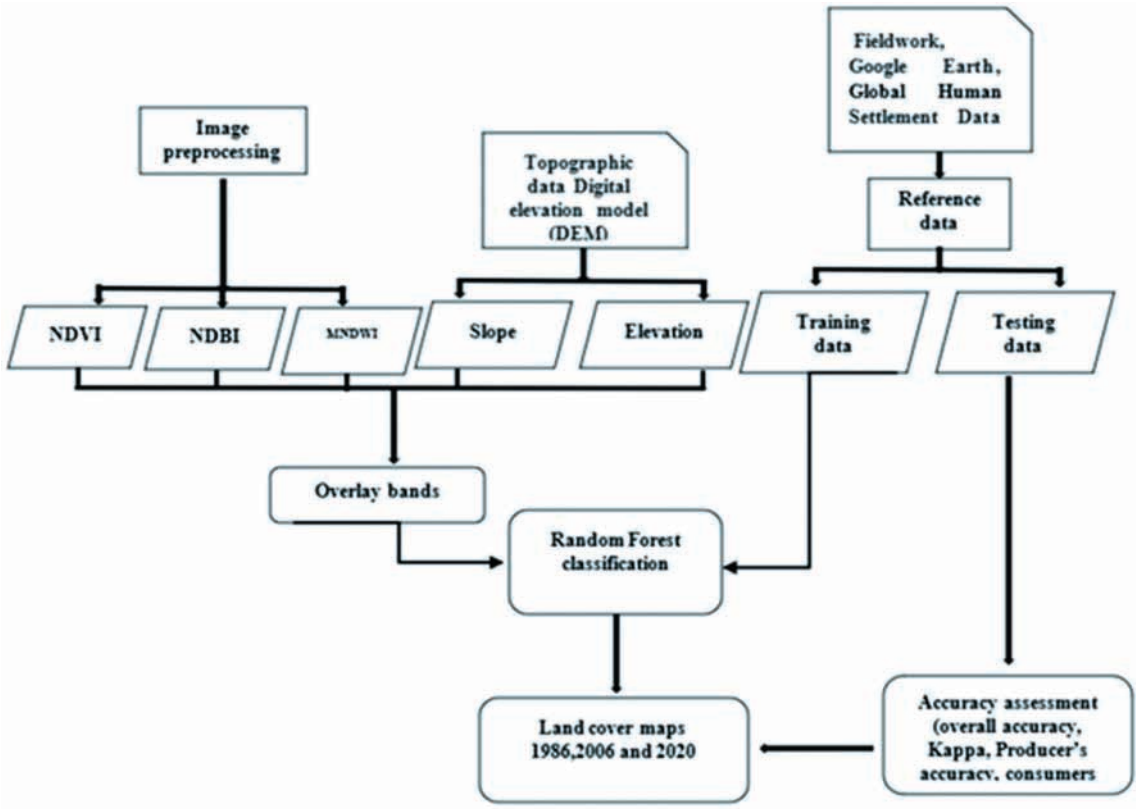

Figure 2. The procedures used for the LULC classification map.

Table 3. Spectral and topographic features.

Type of features	Feature Name
Spectral Bands	Blue, green, red, NIR, SWIR
Indices	NDVI, NDBI, MNDWI
Terrain	Elevation, slope

and 2020, respectively. Random Forest algorithm is a method using tree-type classifiers {h(x,Hk), k = 1,. . .,} where the "Hk" stands for independent identically distributed random vectors and "x" stands for an input pattern (Breiman, 2001). In training, the RF algorithm creates multiple CART-like trees, each trained on a bootstrapped sample of the original training data. It determines a split by examining a randomly selected subset of the input variables (Gislason et al., 2006). In the classification process, each tree provides a unit vote for the most popular class at input x, and the classification of each tree is referred to as a "vote" for that class (A. D. Kulkarni & Lowe, 2016). A complete mathematical presentation of RF is presented by Breiman (2001). The two important parameters the user must optimize to get more accurate results are the number of trees (*Ntree*) generated and the number of features randomly chosen to divide each node (*Mtry*). Based on the pretests from our data, the number of trees was set to 100, and Mtry was set to the default value (square root of the total number of features). Five LULC classes were used in the classification, namely (1) settlement, (2) water, (3) vegetation, (4) agricultural areas (5) bareground. The details are specified in Table 4. The same LULC classes were used for both watersheds to enable the analysis and comparison of the trends between the two watersheds. The choice of these five classes was based on information from key stakeholders in each watershed and followed the trend of previous regional studies, which employed comparable classes (Faty, 2017; Thiam et al., 2022). To perform RF, samples for each class were taken from Google Earth. These samples were used as regions of interest (ROI) to train the RF. Each ROI was given a certain LULC class designation. 70% of the sample was used for training, while 30% was used for internal model validation.

Classification accuracy

Assessing the reliability of the classification results is essential in remote sensing applications. Many researchers recommend using a confusion matrix (Table 5), as well as the accuracy indicators derived from the confusion matrix, including overall accuracy (OA), user accuracy (UO), and producer accuracy (PO) to represent accuracy (Foody Giles, 2022; Szantoi et al., 2021). These indicators show the agreement between the LULC classification results and the actual LULC (Olofsson et al., 2014). In this study, a confusion matrix was generated in GEE. OA (4), UA (5), and PO (6) and kappa index (KA) (7) were then used to evaluate the reliability of the classification

Table 4. Description of the five classes used in the study.

Class	Name	Description
1	Settlement	The human (urban and rural) settlement, housing, roads, transport, mining, and industry.
2	Water	Rivers, streams, ponds, lakes, reservoirs, estuaries, and wetlands,
3	Vegetation	Forest, savannah, riparian vegetation and mixed forest, and mixed forest land.
4	Agriculture area	Agriculture area (irrigated crops, rainfed crops), Pasture.
5	Bareground	Deserts, sand fields, exposed bareground rock, sand and temporary bare ground, transitional areas, mixed barren land.

(Table A1). All these indices (4,5,6,7) take values between 0 (indicating disagreement) and 1 (indicating perfect agreement)). A value above 0.80 for the KA is considered satisfactory (Stehman, 2014).

$$OA_i = \sum_{j=1}^{q} \mathrm{Pjj} \tag{4}$$

$$UO_i = \frac{\mathrm{Pii}}{\mathrm{Pi}} \tag{5}$$

$$PO_i = \frac{\mathrm{Pjj}}{\mathrm{Pj}} \tag{6}$$

$$K_i = \frac{\mathrm{N}\sum_{i=1}^{q}\mathrm{Pii} - \sum_{i=1}^{q}(\mathrm{Pi} + *\mathrm{P} + \mathrm{i})}{\mathrm{N}^2 - \sum_{i=1}^{q}(\mathrm{Ni} + \mathrm{N} + \mathrm{i})} \tag{7}$$

P = number pixels

Land use land cover change prediction

This study used the MLP-MC model embedded in the LCM to simulate future LULC maps. The prediction of future LULC was done in five steps: change analysis, identification of explanatory variables, creation of transition potential maps, change prediction, and validation. LULC maps of the years 1986 and 2006 were employed to analyze the trend of change, to calculate transition potential maps and to predict the LULC map of 2020. For model validation, the LULC map for 2020 was compared with the predicted LULC map of 2020. After demonstrating our model's ability to predict the LULC map of 2020, the same simulation technique was used to predict the LULC maps of 2050 using the LULC maps of 1986 and 2020 based on the business as usual (BAU) scenario (J. Mas et al., 2014). The BAU scenario is a scenario in which future LULC distributions follow the trends observed in the past and are formulated based on the transition probabilities and driving factors as predicted by the model. We assume that the climate will not disrupt human activities. The general scheme of the study is presented in Figure 3.

Table 5. Typical confusion matrix for classification validation (This table has been adapted from Roland (2021)).

Classes	1	2	…	k	…	q	Total
1	P_{11}	P_{12}	…	P_{1k}	…	P_{1q}	P_{1+}
2	P_{21}	P_{22}	…	P_{2k}	…	P_{2q}	P_{1+}
…	…	…	…	…	…	…	…
K	P_{k1}	P_{k2}	…	P_{kk}	…	P_{kq}	P_{k+}
…	…	…	…	…	…	…	…
q	P_{q1}	P_{q1}	…	P_{qk}	…	P_{qq}	P_{q+}
Total	P_{+1}	P_{+2}	…	P_{+k}	…	P_{+q}	P

Changes analysis

The first step was the change analysis to define the transition classes. Changes are described as transitions from one class of LULC to another (Azari et al., 2022). The change analysis was performed by using the two earlier LULC maps with the module change analysis in LCM. The module change analysis estimates the gains and losses of each class between the two earlier LULC maps. Changes in terms of loss (Lij) and gain (Gij) are calculated using equations (8) and (9) (Thiam et al., 2021).

$$\mathrm{Lij} = (\mathrm{Pi} - \mathrm{Pii})\left(\frac{\mathrm{Pj}}{\sum \mathrm{j} = 1\mathrm{Pj}}\right), \quad \text{where } \mathrm{i} \neq \mathrm{j} \tag{8}$$

$$\mathrm{Gij} = (\mathrm{Pj} - \mathrm{Pjj})\left(\frac{\mathrm{Pi}}{\sum \mathrm{i} = 1\mathrm{Pi}}\right), \quad \text{where } \mathrm{i} \neq \mathrm{j} \tag{9}$$

where Lij is the proportion of loss from category i to j under random processes of loss, Pii is the proportion of category i that showed persistence between the two times, Gij is the proportion of gain from category i to j, Pj is the proportion of the landscape in category j at the end of time, Pjj is the observed persistent proportion of category j, and Pi is the entire area of category i at the starting point.

Identification of the explanatory variables

The second step was the identification of the explanatory variables that have driven past LULC changes. Based on the literature, we selected slope, elevation, distance to the river, distance to the settlement, and distance to the road as the main variables influencing the change in LULC over time (Chinwendu, 2019; Murgante et al., 2014). Slope and distance to the river were used to represent the accessibility of a neighbourhood. Distance to road and distance to settlement were selected to highlight the proximity of urbanization.

Transition potential modelling

The third step was the determination of transition potential maps with the multilayer perceptron (MLP) model in LCM. MLP is composed of a neural network

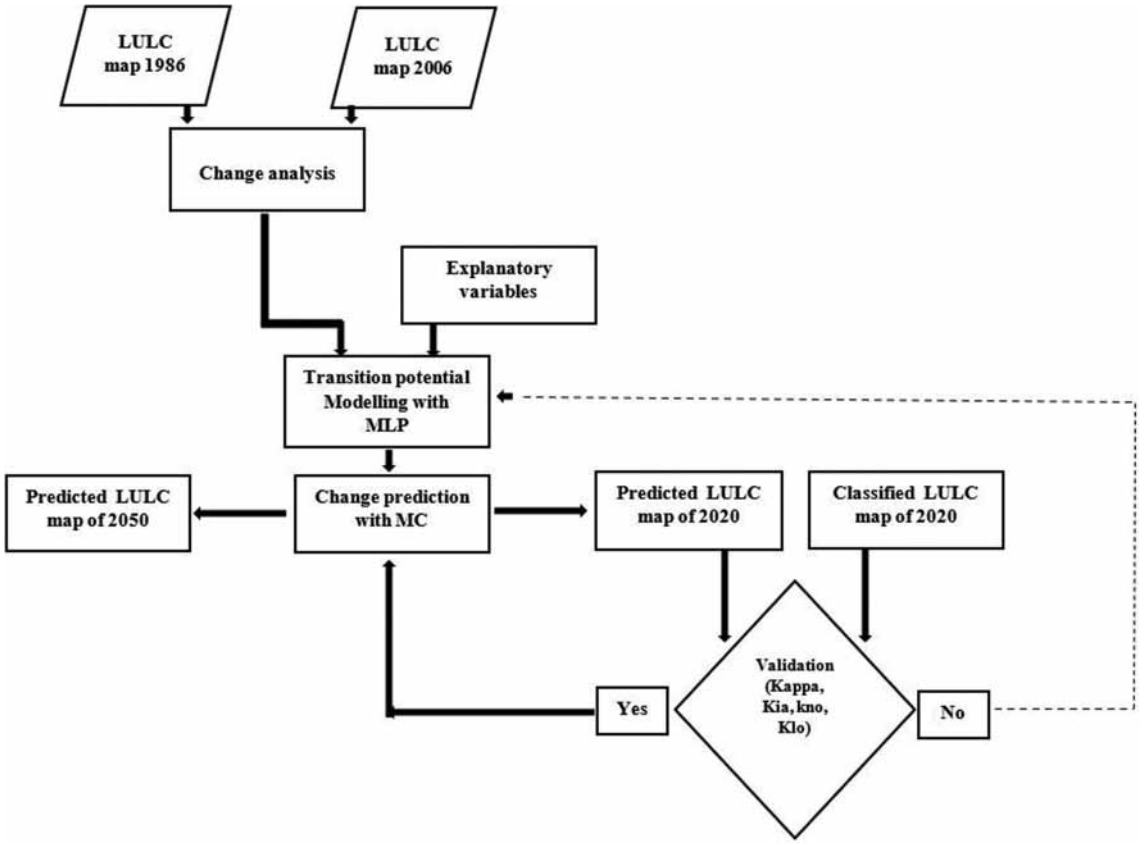

Figure 3. The procedures used to simulate the future LULC map.

based on a feed-forward algorithm with three layers: the input, hidden, and output layers (J. F. Mas & Flores, 2008). MLP adjust the weights of the input and output layers using the backpropagation process. It only incorporates conductive factors with strong predictive capacity into the computation procedure, resulting in different transition potential maps for each submodel. These maps show the ability to change from one LULC class to another (V. Mishra et al., 2014). The MLP model was trained and tested using the explanatory variables and the change analysis obtained between the two earlier images as input. The MLP first created a random sample of cells that transitioned among LULC classes during the required time and started the automatic training process. The sample is divided into two equal parts, 50% of the sample for training and the remaining 50% for testing the performance. Transition potential maps were generated after the successful execution of MLP training for each class.

Change prediction

The fourth step was using Markov Chain (MC) in LCM to predict the LULC map for a specified future date. The historical rate change determined during the change analysis phase and transition potential maps are used as input in the MC model to predict the future LULC. The MC model is a stochastic process that shows the probability that one state will change into another. The MC model uses this information as the basis to predict future changes. By examining past changes, MC model creates a transition probability matrix of changes (V. N. Mishra et al., 2018). Based on a projection of the transition potentials into the future, the technique estimates precisely the amount of LULC expected to transition from the later date to the predicted date and provides a transition probability file.

Validation

The validation process aims to verify the accuracy of the predicted map compared to a reference map. The validation process in LCM involves cross-tabulation in a three-way comparison between the later LULC map, the predicted LULC map, and the actual map. Two approaches have been used for model validation. The first approach is to use the metric performance indicators relative operational characteristic (ROC) and the validation statistics of various Kappa indices (Kappa for no information (Kno), Kappa for location (denoted Klocation), KIA for Kstandard) between the classified map and the predicted 2020 map to assess the accuracy of the prediction (Pontius & Batchu, 2003). A LULC model is valid if the Kstandard is greater than 70%, according to Zadbagher et al. (2018). The second approach is to compare the predicted and actual area of each LULC class.

Results

Land use land cover maps accuracy

This section presents the results of LULC classification for the two watersheds. Figures 4, 5, 6 and 7 show the results of the independently classified images for 1986, 2006 and 2020. Table 6 presents the classification accuracies. The overall accuracy is equal to 96%, 95% and 95% for 1986, 2006 and 2020, respectively. All these indices (user accuracy (UA), and producer accuracy (PA)) take values between 0.75 and 0.98 (indicating perfect agreement). The Kappa index obtained for both maps is above the threshold of 0.8. A value above 0.80 is considered satisfactory (Olofsson et al., 2014; Szantoi et al., 2021). Therefore, the classification could be identified as accurate.

Land use land cover change detection

Bafing

According to Figures 4 and 5, in 1986, the area covered by bareground was the most dominant LULC class, covering 60% of the watershed. Over the 34 years, this area has gradually decreased to almost half, from 60% to 30%. The vegetation area represents the second most dominant LULC class, covering 36% of the watershed. This class has continuously increased from 36% in 1986 to 44% in 2020. Settlement were the third most dominant LULC class and covered 2.8% in 1986. However, settlement significantly increased to 16% in 2006 and 18% in 2020. The agricultural areas were the fourth LULC class, covering 0.8% of 1986 in the watershed. The extent of agricultural areas increased from 0.8% in 1986 to 4% in 2020. The area covered by water was the lowest but increased continuously over the study period from 0.6% to 3.3%.

Faleme

Analysis of the LULC map of 1986 (Figures 6 and 7) shows a predominance of bareground, representing an area of 78% in the watershed. Overall, the area covered by bareground continuously decreased from 78% to 44% during the study period. Vegetation were the second most dominant LULC class, covering 20% in 1986, as in Bafing. However, the extent of vegetation area increased from 20% to 28% in 2006 and decreased from 28% to 23% in 2020. Settlement were the third most dominant LULC class, with an area of 1.7% in 1986. Settlement class increased steadily to

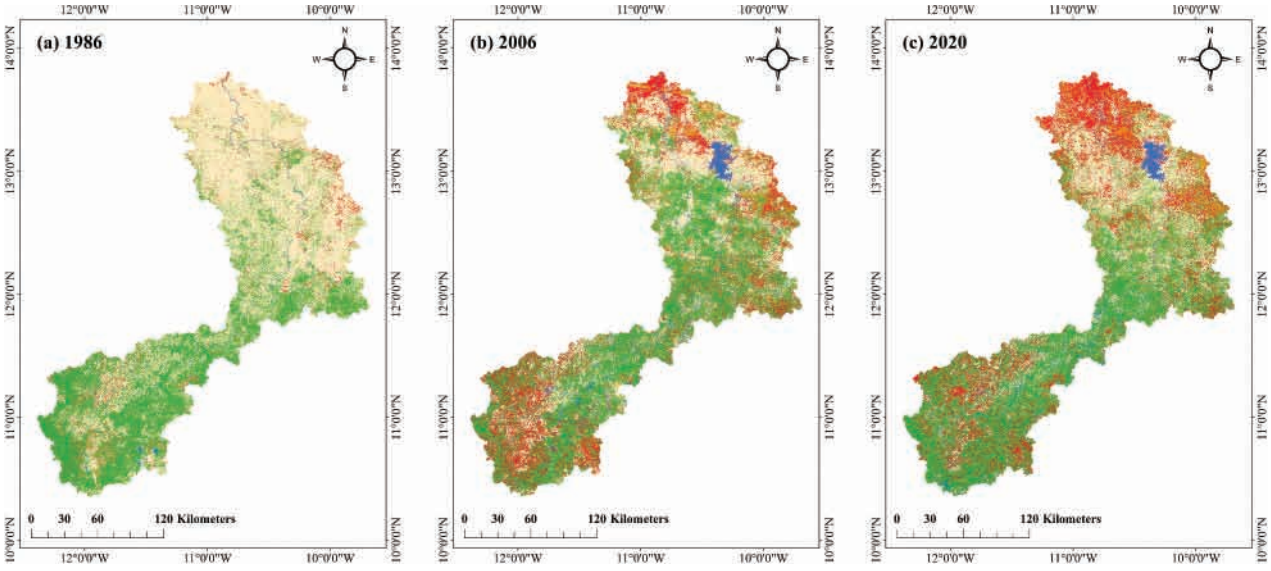

Figure 4. LULC maps of the Bafing for the years a) 1986, b) 2006, and c) 2020.

		LULC Types_Bafing		
Classe	Name	1986	2006	2020
1	Settlement	2.77	15.95	17.93
2	water	0.59	2.87	3.3
3	vegetation	35.66	42.73	43.85
4	cultivated_area	0.83	3.97	4.04
5	Bare ground	60.15	34.47	30.87
	Total	100	100	100

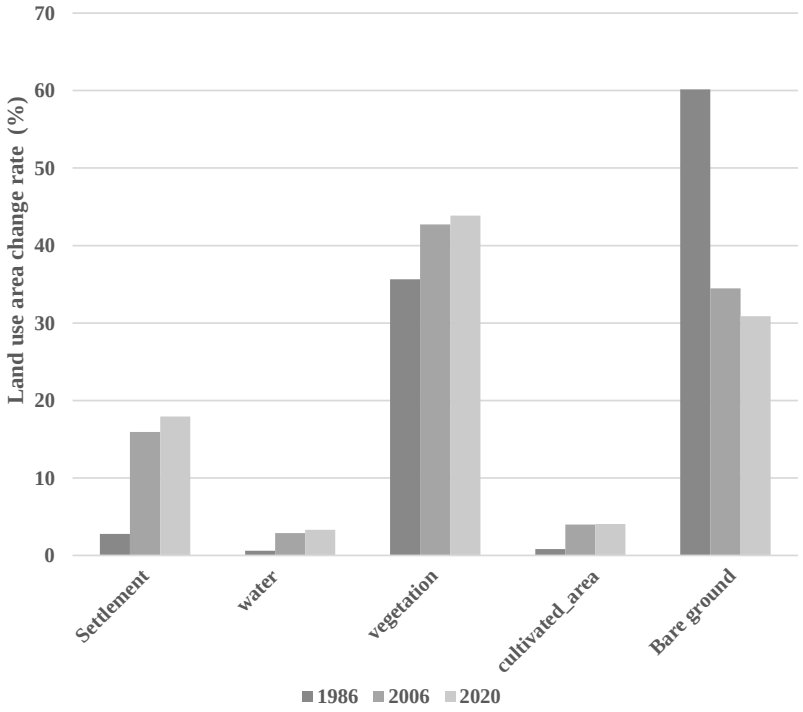

Figure 5. Percentage of area per LULC category for 1986, 2006, and 2020.

10% in 2006 and 28% in 2020, becoming the second most dominant LULC class. Between 1986 and 2020, the area covered by water increased from 0.46% in 1986 to 1.3% in 2006 but decreased from 1.3% (in 2006) to 1.1% in 2020. The agricultural areas represented the lowest coverage, covering less than 0.2% of the watershed in 1986 but increasing markedly from 0.2% to 4.7% in 2006. However, the agricultural areas class showed a downwards trend between 2006 and 2020, from 4.7% to 3.5% in 2020.

Land use land cover change prediction

Transition potential

The most significant surface state changes were analyzed between 1986, 2006 and 2020 to select the dominant changes in the modelling procedure. From 1986 to 2006 and from 2006 to 2020, conversions from bareground to vegetation, settlement, agricultural areas, and water were the most significant for Bafing. For Faleme, the overall distribution results for 1986, 2006, and 2020 showed that the most significant

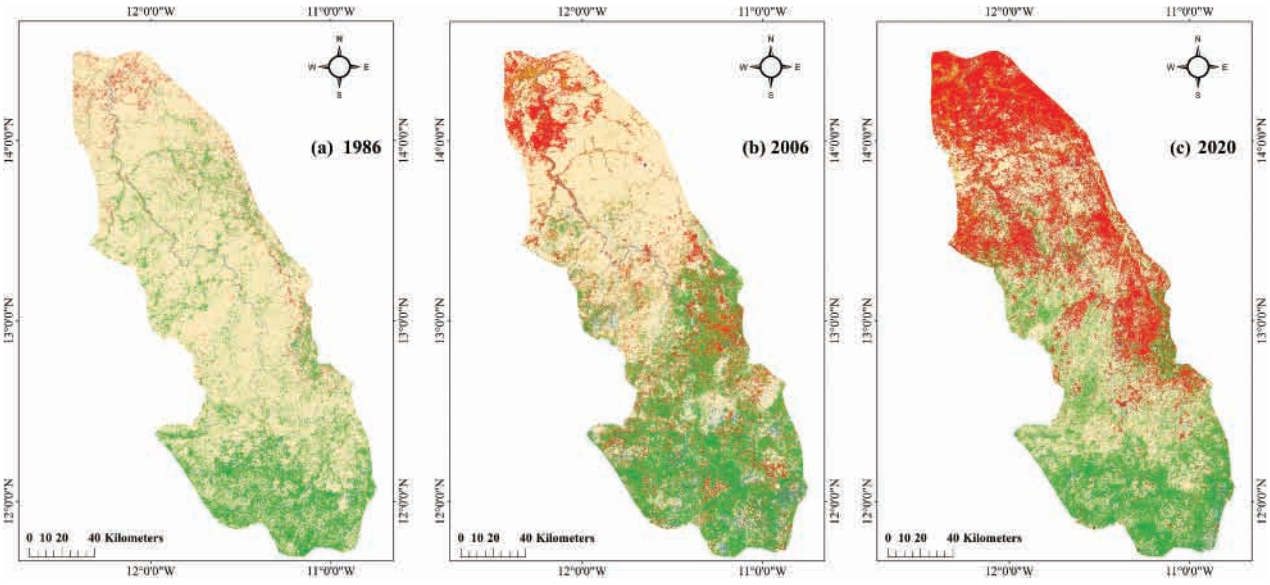

Figure 6. LULC maps of the Faleme for the years 1986, 2006, and 2020.

		LULC Types_Faleme		
Classe	Name	1986	2006	2020
1	Settlement	1.7	10.15	27.88
2	water	0.46	1.33	1.09
3	vegetation	19.62	27.77	23.22
4	cultivated_area	0.2	4.71	3.54
5	Bare ground	78.02	56.05	44.28
	Total	100	100	100

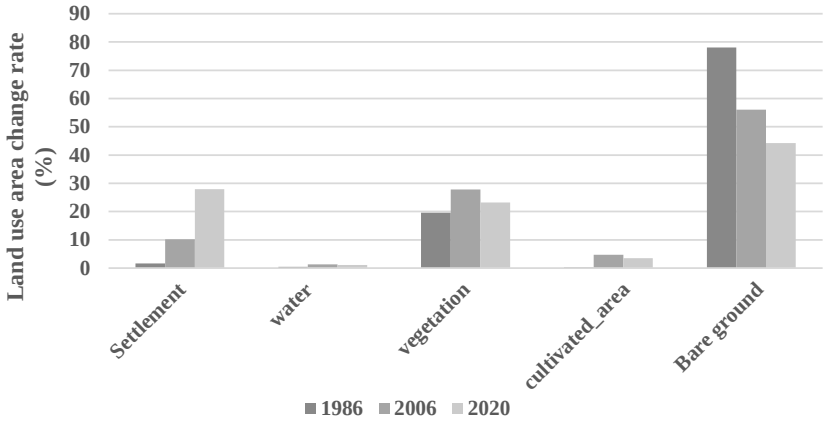

Figure 7. Percentage of area per LULC category for 1986, 2006, 2020.

Table 6. Classification accuracies: user's accuracy (U.A), producer's accuracy (P.A), overall accuracy (O.A) and the Kappa accuracy (K.A) for each of the selected images.

	1986		2006		2020	
Landcover/land use class	PA	UA	PA	UA	PA	UA
Settlement	0.84	0.96	0.94	0.93	0.97	0.95
Water	0.99	0.99	0.98	0.99	0.93	0.96
Vegetation	0.99	0.99	0.98	0.96	0.96	0.95
Agricultural areas	0.75	0.87	0.90	0.97	0.85	0.93
Bareground	0.98	0.95	0.97	0.94	0.96	0.95
Overall accuracy (O.A)	0.96		0.95		0.95	
Kappa accuracy (K.A)	0.95		0.94		0.94	

changes for the period (1986–2006) were transitions from bareground to settlement, agricultural areas, vegetation, and water. Over 2006 and 2020, conversions from vegetation and bareground to all other classes, including water, agricultural areas and settlement, were the most significant.

Model validation

Bafing. On the simulated LULC map of 2020 (Figure 8b), the areas occupied by settlement, vegetation, bareground, water and agricultural areas are 18.75%, 44.76%, 28.50%, 3.91%, and 4.08%, respectively, against 17.93%, 43.85%, 30.87%, 3.30%, and 4.04%, respectively, on the reference map of 2020 (Figure 8a).

Figure 10 shows no significant difference between the simulated and predicted areas. The visual comparison of the simulated 2020 map with the actual map is reasonably similar. In addition, the validation indicators provide values of ROC = 81.6%, κia (kstandard) = 78.34%, Klo = 79.86% and kno = 86.83% (reflecting the overall accuracy of the simulated map), which are considered satisfactory (Chinwendu, 2019; Olofsson et al., 2014; Roland, 2021; Tiné et al., 2019). These results indicate that the MLP- CA model reasonably simulated the LULC map of 2020 and can be used to project future LULCC in Bafing.

Faleme. On the simulated LULC map of 2020 (Figure 9b), the areas occupied by settlement, water, vegetation, agricultural areas and bareground are 11.10%, 1.73%, 30.10%, 5.88% and 51.20%, respectively, compared to 27.88%, 1.09%, 23.22%, 3.54% and 44.28%, respectively, on the reference map of 2020 (Figure 9a). There is a significant difference between the observed and predicted areas. This difference is due to the change in trend described above between the period 1986–2006 and the period 2007–

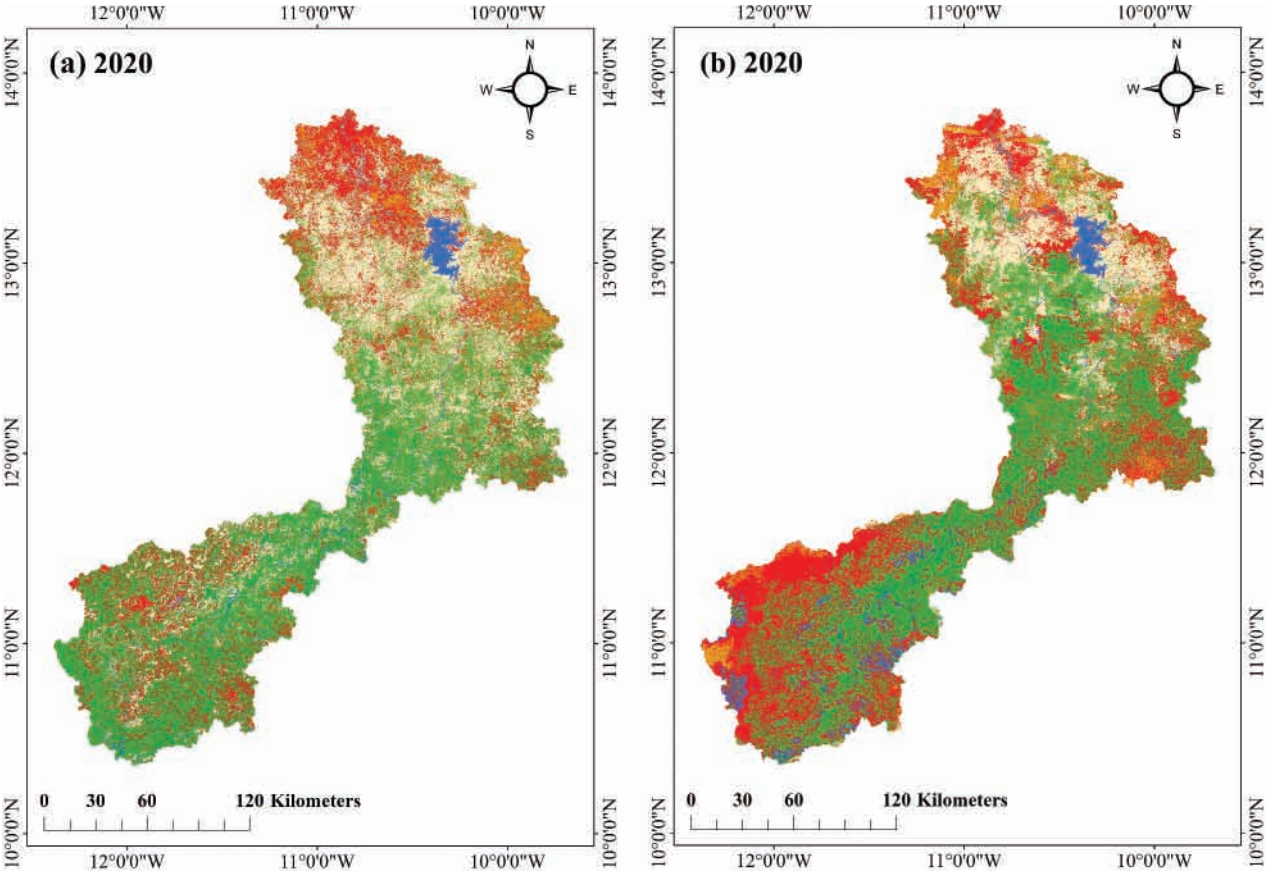

Figure 8. Comparison of the Reference and Simulated Maps of Bafing for 2020.

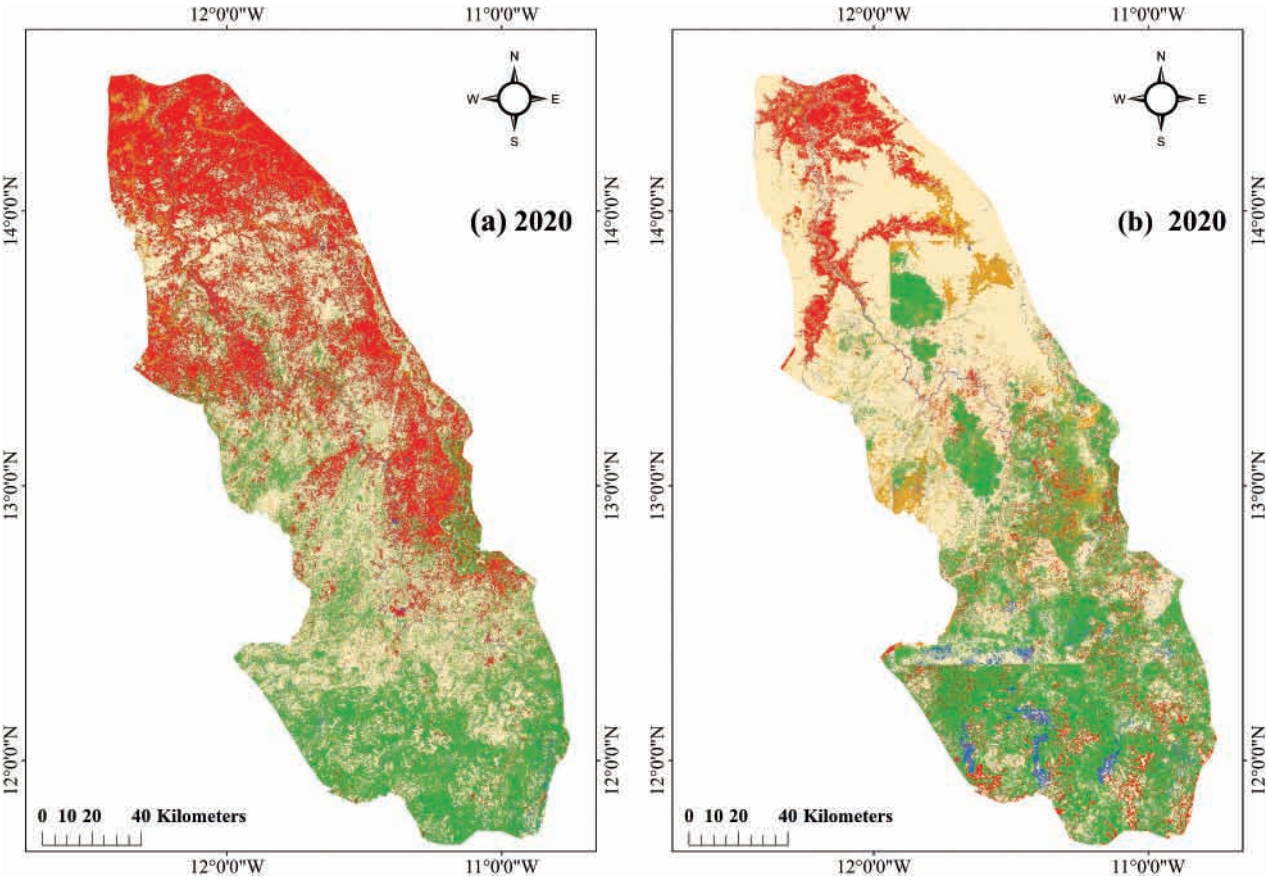

Figure 9. Comparison of reference and simulated LULC 2020 maps of Faleme.

2020. Although the validation indicators provide values of ROC = 75.92%, κia (kstandard) = 0.58%, Klo = 67.14% and kno = 67.14%, (reflecting the overall accuracy of the simulated map) deemed fair (Chinwendu, 2019; Olofsson et al., 2014; Roland, 2021; Tiné et al., 2019), the simulated maps for 2020 cannot be considered satisfactory. Thus, our model cannot be validated for the Faleme. Nevertheless, we have produced the simulated LULC map for 2050 based on the trend (2006–2020) that describes the current development in Faleme.

Projected LULC maps

For Bafing, changes in LULC between 1986 and 2020 were first analyzed, leading to transition potential maps and a probability matrix illustrating the significant LULCC. The transition probability matrix for the classified maps is presented in Table 7. Analysis of the Table 7 results shows that between 1986 and 2020, the settlement, agricultural areas, and bareground classes were the most dynamic. Indeed, the settlement and agricultural areas classes indicate a 45% and 18% probability of not changing to another LULC class, respectively. At the same time, the area of agricultural areas and bareground has a probability of 23.6% and 219% of transforming into settlement. Similarly, the vegetation class also shows stability with a chance of 80.7%. Bareground have a high possibility of turning into vegetation at 22%.

Finally, the LULC projection scenarios for Bafing in 2050 were simulated based on the probability matrix obtained using the 1986 and 2020 maps. Figure 10 shows the predicted LULC maps for 2050. The results of this simulation indicate that vegetation will cover the largest area with 49% in 2050, followed by settlement with an area of 19%. Bareground will be the third most dominant LULC class and will cover 22% in 2050. Water and agricultural areas will each cover 4.8% of the area.

For Faleme (Figure 10), based on the probability matrix obtained using the 2006 and 2020 maps, the simulation results show an increase in settlement areas, and agricultural areas will be observed by 2050. There is also a decrease in water, vegetation, and bareground.

Discussion

The global environment changes are acknowledged to be fundamentally and significantly influenced by LULC changes. This study aimed to evaluate LULCC over 34 years in two watersheds (Bafing and Faleme) of the SRB and to simulate future changes in LULC in 2050 with the status quo (BAU) assumption. This study used the RF classification algorithm and Landsat images from 1986, 2006 and 2020 for the LULC mapping. RF classification results are very satisfactory with good accuracy. We noticed that some pixels are poorly classified, especially in Faleme. This confirms the results of Zurqani et al. (2018), who suggest that the RF algorithm works better in areas where LULC types are dominated by vegetation. The analysis of the post-classification change detection has reported significant changes in LULC during the study period.

Analysis of changes in Bafing between 1986 and 2020 revealed the expansion of settlement and agricultural areas at the expense of bareground. These results corroborate those of Herrmann et al. (2020), who proved that the intensity of LULC change in settlement and agricultural areas was high in WA. Studies have showed that the increase in settlement and agricultural areas is caused by the increasing population in the WA (Assede et al., 2023). Indeed, the average growth rates are 2.5% and 2.7% for the countries covering our study areas, namely, Guinea and Mali. Tabutin and Schoumaker (2020) observed a high population rate in WA and the resulting socio-economic impacts (increase in agricultural areas). These results also mirror those of Berihun et al. (2019), who also found that population increase was consistent and positively correlated with the expansion of agricultural areas between 1982 and 2006 in Ethiopia. The results on the increase in vegetation during 1986–2020 are in good agreement with the findings of previous studies conducted in Fouta Djallon Plateau of Bafing in Guinea. Indeed, These results are consistent with the results of UCAD (2019) and Descroix et al. (2020), who found a regreening in Fouta Djallon Plateau of Bafing in Guinea. The increase in vegetation that coincides with population growth suggests that population growth does not always lead to deforestation. Indeed, Descroix et al. (2020) pointed out that the densely populated areas of the Fouta Djallon Plateau of Bafing in Guinea are those where the vegetation cover is not threatened and where the ecological intensification of rural activities has long been established. Therefore, the claim "more people, more trees"

Table 7. Transition probability matrix (%) of the LULC map for the period from 1986 to 2006 of Bafing.

Bafing makana	Settlement	Water	Vegetation	Agriculture area	Bareground
Settlement	**0.4515**	0.0158	0.2527	0.1149	0.165
Water	0.0491	**0.06236**	0.2236	0.0014	0.1024
Vegetation	0.0796	0.0358	**0.8065**	0.0139	0.13
Agriculture area	0.2364	0.0544	0.4893	**0.1813**	0.3122
Bareground	0.2089	0.0216	0.2157	0.0471	**0.6836**

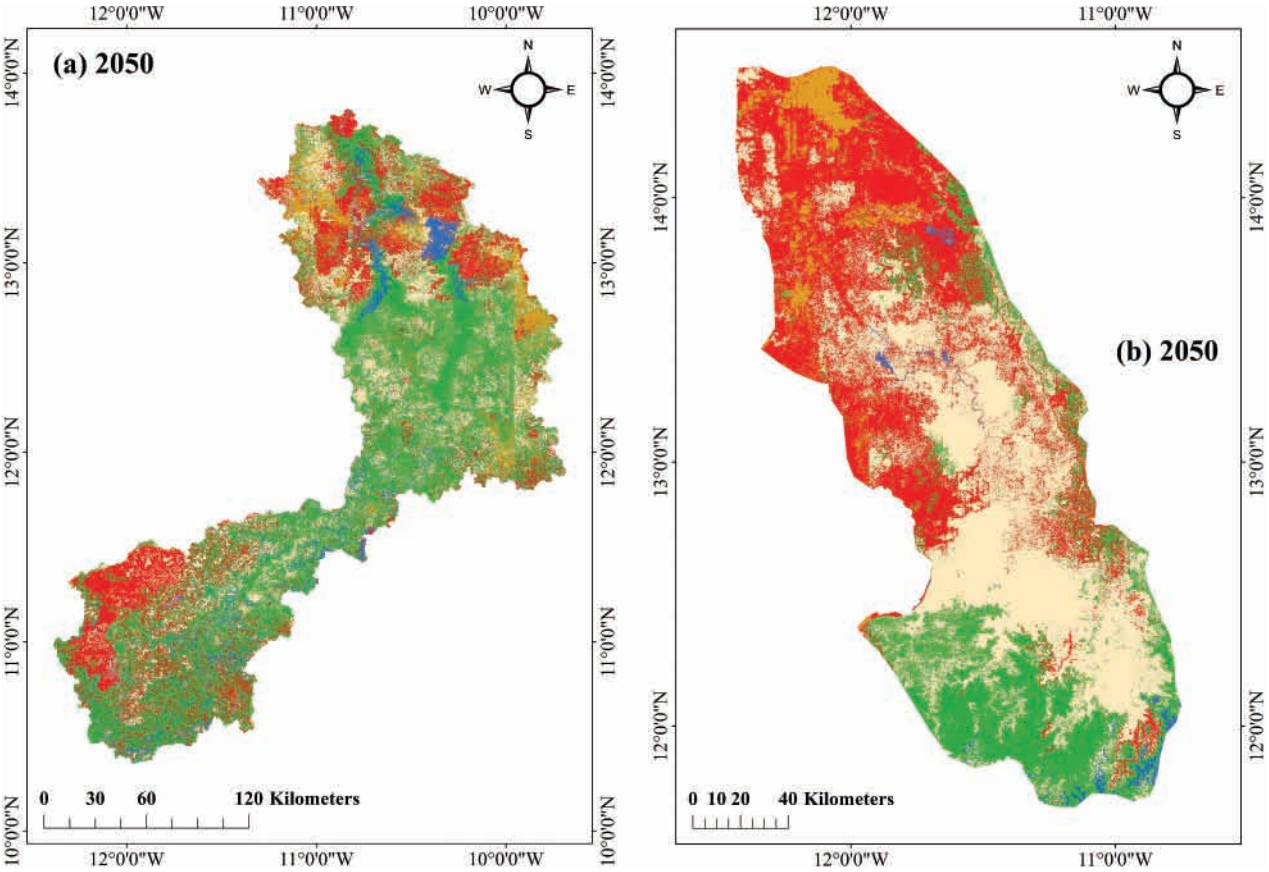

Figure 10. Predicted LULC maps 2050 of a) Bafing and b) Faleme.

proposed in Tanzania by Kabanza et al. (2013) seems valid for Bafing. In addition, it should be noted that several projects have been adopted in the Bafing in Mali to fight biodiversity losses after the construction of the Manantali Dam. Among these projects, we can mention the Bafing Faunal Reserve (Mali), the status of biosphere reserve (Mali), the Natural Resources Management Project (PGRN/World Bank) in the 1990s and 2000s, the Project for the Extension and Strengthening of Protected Area Systems, the Bafing transboundary area protected area project during the period 2010–2015 (Faty, 2017). Another significant result obtained is the increase in water between 1986 and 2020. The observed increase in water can be explained by the recovery of rainfall in this region in the 1990s, after the drought period of 1960–1970. Several authors (Bodian et al., 2020; Diop et al., 2016; Nouaceur et al., 2020) noted a recovery in rainfall in WA. Bodian et al. (2020) studied the recent evolution of hydroclimatic variables in the SRB from 1940 to 2013. These results show a recovery in annual rainfall in the SRB, which improves surface water availability. Recovery of annual flow was reported after the 1990s in Bafing (at Bafing Makana station) (Sane et al., 2017). It can also be attributed to the construction of the Manantali dam in Bafing. The Manantali Dam, built in 1988, has an area of approximately 477 km2 and a capacity of 11,791.8 million m^3 (Bader, 2001). It aims to make surface water available and sustainable throughout the year and to satisfy energy production and flow regulation, especially in the context of climate change and variability (Bader et al., 2015).

In Faleme, the analysis of the post-classification change detection revealed that areas occupied by settlement increased from 1986 to 2020. The results also show that agricultural areas, vegetation and water increased significantly between 1986 and 2006. However, there was a decrease in agricultural areas, vegetation, and water between 2006 and 2020. These results can be explained by the artisanal extraction of gold in Faleme during the last decades. Overpopulation in Faleme is strongly linked to population growth and mining activities (industrial and artisanal). Faleme supports the gold resources of eastern Senegal and Mali Artisanal gold mining has increased significantly in recent decades, mainly due to the rising price of gold on the international market and the difficult socioeconomic situation (Bohbot, 2017). Artisanal gold mining is becoming a profession like agriculture and livestock in Faleme (Ministry of Economy and Finance,2018). This activity generates several sources of income in the different localities where it is practised, but it also causes several environmental impacts, including on soils, water resources and deforestation (Bohbot, 2017). The results of this study on Faleme are in good agreement

with the conclusions of previous studies conducted in regions where gold panning is practiced. For example, results on the decrease in agricultural areas in Faleme are consistent with those of Atteyoub and Camara (2020) and Ndiaye (2020) who reported that the development of gold panning has led to the gradual abandonment of agricultural practice in this area. Similarly, Doucouré (2015) in his book "Des pierres dans les mortiers et non du maïs! Mutations in the gold-mining villages of southeastern Senegal", describes the abandonment of agricultural areas in favor of gold panning. The deforestation and reduced water surface quality in Faleme is also consistent with the results of Traoré (2022) at kenieba in Mali and at Nzema in Ghana Kaku et al. (2021).

The predicted LULC map of 2050 was performed using the MLP-MC model embedded in LCM with the BAU scenario. LULCCs prediction involves two different aspects. The first is the amount of change, and the second is the spatial distribution of change. LCM provides the amount of change by comparing initial (1986) and second (2006) LULC maps with the MLP and then predicting future land cover (2020) using the MC transition probability matrix for the future. Model validation is performed by comparing the simulated LULC map (2020) with the classifier LULC map (2020)'. For Bafing, the model has been validated with satisfactory results. The simulation results indicate that the observed and predicted LULC map of 2020 were in good agreement. During the period 2020–2050, the prediction results (based on the past trend (1986–2020) revealed that vegetation would be the dominant LULC, but an increase in agricultural areas, water, and settlement will also be observed in 2050.

For Faleme, the model has not been validated with satisfactory results. The results showed that the observed and simulated LULC maps of 2020 were not in good agreement, and errors for all classes were noted. These results can be explained by the trend shift between the previously mentioned periods (1986–2006) and (2007–2020). The results of the validation of the MLP_MC model on the Faleme showed a limitation of deterministic prediction models such as MLP_MC in LCM. The principle behind MLP- MC projections is that the rates of change observed during the calibration phase will remain unchanged during the simulation period, which in many circumstances, is an incorrect assumption, according to J. Mas et al. (2014). Approaches based on historical tendencies may or may not be effective. The predicted LULC map 2050 was then obtained based on LULC changes from 2006 to 2020. The results indicated that the settlement area increased from 10.15% to 27.88% from 2006 to 2020, and the prediction results confirm that it will continue to expand to 32.58% during 2020–2050, at the cost of a reduction in vegetation (23.22% to 19.83%). Such a loss of vegetation is expected to reach a critical threshold in the coming years, showing the need to develop better spatial planning and adapted sustainable development strategies. These combinations of results suggest that population growth and anthropogenic activities appear to be the primary driver of LULC changes in these two watersheds.

These two watersheds show that while population growth can contribute to increased pressure on land resources and lead to unsustainable land-use practices, it is not the only determinant of these issues. Other factors, such as socioeconomic activities, agricultural practices, appropriate policies and regulations, education and awareness, also play an essential role. The results in Bafing showed that when population growth is accompanied by adopting sustainable land management practices, it can lead to better land and water conservation. The presence of a large dam in Bafing has led to the implementation of virtuous policies favourable to the environment. In Faleme, mining activities, many of which are uncontrolled, are leading to environmental degradation. These divergent development trajectories have different impacts on the water cycle and must be considered in water development policies for the Senegal River basin.

The main limitation of our study is that it did not consider stakeholder involvement in LULCC modelling processes. According to Hewitt et al. (2014), the information of stakeholders on LULCC drivers, reconstruction of timelines of major past events and their perspective on potential future trajectories of land-use change are essential to achieve holistic results in a participatory manner and complement model results. This technique bridges the gap between practitioners' perspectives and those of technical or policy stakeholders (Thiam et al., 2022). In addition, the use of hybrid prediction models integrating several individual models could improve the prediction and allow the simulation of LULCC to be more realistic (Gaur et al., 2020; Girma et al., 2022; Sankarrao et al., 2021). Sankarrao et al. (2021) compare different LULCC modelling techniques to predict the future LULC by testing MLP-MC, Logistic Regression-Markov Model (LR-MC), Multilayer Perceptron Markov Chain Cellular Automata (MLP_MC_CA) and Logistic Regression Markov Model Cellular Automata (LR_MC_CA) models on Nagavali River Basin (NRB), in Southern India. The results revealed that after combining the MLP_MC model with the Cellular Automata, the model was improved in terms of the Kappa coefficient. In addition, the hybrid model MLP-MC-CA had a better agreement than the other models. Furthermore, the study did not incorporate climate change and variability drivers.

Considering these limitations, future research can fill the gaps left by these shortcomings. This work was done to establish scenarios for the construction of hydropower dams and to assess the combined effects of LULC and climate change on the services these dams will provide in these watersheds (Sambou et al., 2023). This document allows the OMVS to develop adequate land and water resource management policies and strategies specific to each watershed, considering the sustainable development goals.

Conclusion

This study analyzed the historical LULCC from 1986 to 2020 with the RF classification and the projected LULC for 2050 by using the MLP-MC model in the Bafing and Faleme in the SRB. The main results revealed that spatial and temporal changes have occurred. During 1986–2020, a significant increase in vegetation, water, agricultural areas and settlement and a decrease in bareground were found in Bafing. The projections of LULC for 2050 show effect for the environment by the increase in vegetation, agricultural areas and settlement. The analysis in Faleme show an increase in settlement, vegetation, agricultural areas, and water, as well as a decrease in bareground between 1986 and 2006. Between 2006 and 2020, settlement increased. However, there was a decline in vegetation, agricultural areas, water, and bareground. By 2050 (based on 2006–2020 trends), land use changes will convert in a direction incompatible with a balanced environment. The analysis of surface state dynamics revealed that population growth and changing anthropogenic (socioeconomic) activities were the main drivers of LULC changes. The changes in LULC are both positive and negative. Based on LULCC, the SRB experienced a trend towards "more people, more trees" for the Bafing and "more people, more deforestation" for the Faleme. These two examples show that population growth, accompanied by adopting sustainable land management practices, can lead to better water and land conservation. These divergent development pathways have different impacts on the water cycle and must be considered in water development policies for the Senegal river basin.

Disclosure statement

No potential conflict of interest was reported by the author(s).

Funding

This paper is a component of a PhD research financed by the German Federal Ministry of Education and Research (BMBF) and undertaken at the University of Abomey-Calavi, Republic of Benin, on behalf the West African Science Service Center on Climate Change and Adapted Land Use (WASCAL).

ORCID

Zoltan Szantoi http://orcid.org/0000-0003-2580-4382

Data availability statement

The data that support the findings of this study are available from the corresponding author, M H Astou SAMBOU, upon reasonable request.

References

Amini, S., Saber, M., Rabiei Dastjerdi, H., & Homayouni, S. (2022). Urban land use and land cover change analysis using random forest classification of Landsat time series. *Remote Sensing*, *14*(11), 1–23. https://doi.org/10.3390/rs14112654

Andrieu, J. (2018). Land cover changes on the West-African coastline from the Saloum Delta (Senegal) to Rio Geba (Guinea-Bissau) between 1979 and 2015 land cover changes on the West-African coastline from the Saloum Delta. *European Journal of Remote Sensing*, *51*(1), 314–325. https://doi.org/10.1080/22797254.2018.1432295

Anwar, Z., Alam, A., Elahi, N., & Shah, I. (2022). Assessing the trends and drivers of land use land cover change in district Abbottabad lower Himalayan Region Pakistan. *Geocarto International*, *37*(25), 10855–10870. https://doi.org/10.1080/10106049.2022.2040604

Assede, E., Orou, H., Biaou, S., Geldenhuys, C., Ahononga, F., & Chirwa, P. Understanding drivers of land use and land cover change in Africa: A review. (2023). *Landscape Ecol Rep*, *8*(2), 62–72. *(2023)*, 4(1), 88–100. https://doi.org/10.1007/s40823-023-00087-w

Atteyoub, M., & Camara, M. (2020). Impact socioeconomique de l ' orpaillage dans le socio-economic impact of gold panning in the kadiolo. *Revue Malienne de Science et de Technologie*, *01*(24), 91–103.

Azari, M., Billa, L., & Chan, A. (2022). Multi-temporal analysis of past and future land cover change in the highly urbanized state of Selangor, Malaysia. *Ecological Processes*, *11*(1). https://doi.org/10.1186/s13717-021-00350-0

Bader, J. C. (2001). *Programme d'optimisation de la gestion des réservoirs : manuel de gestion du barrage de Diama : version finale*.

Barnieh, B. N. A. I. N. A., Jia, L., Menenti, M., & Zhou, J. (2020). Mapping land use land cover transitions at different Spatiotemporal scales in West Africa. *Sustainability 2020*. https://doi.org/10.3390/su12208565

Berihun, M. L., Tsunekawa, A., Haregeweyn, N., Meshesha, D. T., Adgo, E., Tsubo, M., Masunaga, T., Fenta, A. A., Sultan, D., & Yibeltal, M. (2019). Exploring land use/land cover changes, drivers and their implications in contrasting agro-ecological environments of Ethiopia. *Land Use Policy*, *87*(May), 104052. https://doi.org/10.1016/j.landusepol.2019.104052

Bodian, A., Diop, L., Panthou, G., Dacosta, H., Deme, A., Dezetter, A., Ndiaye, P. M., Diouf, I., & Visch, T. (2020). Recent trend in hydroclimatic conditions in the Senegal River basin. *Water (Switzerland)*, *12*(2), 1–12. https://doi.org/10.3390/w12020436

Bohbot, J. (2017). L'orpaillage au Burkina Faso : une aubaine économique pour les populations, aux conséquences sociales et environnementales mal maîtrisées. *EchoGéo*, *42*(42), 15150. https://doi.org/10.4000/echogeo.15150

Breiman, L. (2001). Random Forests. *Lecture Notes in Computer Science (Including Subseries Lecture Notes in Artificial Intelligence & Lecture Notes in Bioinformatics)*. https://doi.org/10.1007/978-3-030-62008-0_35

Cabral, A. I. R., & Lagos, F. (2017). Land cover changes and landscape pattern dynamics in Senegal and Guinea Bissau borderland. *Applied Geography*, *82*, 115–128. https://doi.org/10.1016/j.apgeog.2017.03.010

Chang, Y., Hou, K., Li, X., Zhang, Y., & Chen, P. (2018). Review of land use and land cover change research progress. *IOP Conference Series: Earth and Environmental Science*, *113*(1). https://doi.org/10.1088/1755-1315/113/1/012087

Chinwendu, O. G. (2019). *Modeling the hydrological response of the dano catchment, in the volta basin to land use land cover*, (B. Sc. Water Resources Management and Agromeotrology, M. *Sc*. Climate Change and Adapted Land use), Kwame Nkrumah University of science, A thesi.

Descroix, L., Faty, B., Manga, S. P., Diedhiou, A. B., Lambert, L. A., Soumaré, S., Andrieu, J., Ogilvie, A., Fall, A., Mahé, G., Diallo, F. B. S., Diallo, A., Diallo, K., Albergel, J., Tanimoun, B. A., Amadou, I., Bader, J. C., Barry, A., Bodian, A. . . . Vandervaere, J. P. (2020). Are the fouta djallon highlands still the water tower of west africa? *Water (Switzerland)*, *12*(11), 2968. https://doi.org/10.3390/w12112968

Diallo, B. A., & Zhengyu, B. A. O. (2018). Land cover change assessment using remote sensing: Case study of Bamako, land cover change assessment using remote sensing: Case study of Bamako, mali. *Researcher*, *2*(4), 7–17.

Diop, L., Bodian, A., & Diallo, D. (2016). Spatiotemporal trend analysis of the mean annual rainfall in Senegal. *European Scientific Journal, ESJ*, *12*(12), 231. https://doi.org/10.19044/esj.2016.v12n12p231

Doucouré, B. (2015). *Des pierres dans les mortiers et non du maïs! Mutations dans les villages aurifères du sud-est du Sénégal*.

Dubertret, F., Villarreal, M. L., Tourneau, F. L., Dubertret, F., An-, L. N. M., Villarreal, M., Tourneau, F. L., Tourneau, F. L., Villarreal, M., & Dubertret, F. (2022). Monitoring annual land use/land cover change in the Tucson metropolitan area with google earth engine (1986–2020). *Remote Sensing*, *14*(9), 2127. https://doi.org/10.3390/rs14092127

Fathizad, H., Rostami, N., & Faramarzi, M. (2015). Detection and prediction of land cover changes using Markov chain model in semi-arid rangeland in western Iran. *Environmental Monitoring and Assessment*, *187*(10). https://doi.org/10.1007/s10661-015-4805-y

Faty, A. (2017). Modelisation hydrologique du haut bassin versant du fleuve senegal dans un contexte de variabilite hydro-climatique : Apport de la télédétection et du modèle Mike SHE. *Université Cheikh Anta Diop de Dakar*.

Fikadu, G., & Olika, G. (2023). Impact of land use land cover change using remote sensing with integration of socio-economic data on rural livelihoods in the Nashe watershed, Ethiopia. *Heliyon*, *9*(3), e13746. https://doi.org/10.1016/j.heliyon.2023.e13746

Foody Giles, M. (2022). Land cover classification accuracy assessment. *Springer Geography*, *80*, 105–118. https://doi.org/10.1007/978-981-16-5149-6_6

Gaur, S., Mittal, A., Bandyopadhyay, A., Holman, I., & Singh, R. (2020). Spatio-temporal analysis of land use and land cover change: A systematic model inter-comparison driven by integrated modelling techniques. *International Journal of Remote Sensing*, *41*(23), 9229–9255. https://doi.org/10.1080/01431161.2020.1815890

Girma, R., Fürst, C., & Moges, A. (2022). Land use land cover change modeling by integrating artificial neural network with cellular Automata-Markov chain model in Gidabo river basin, main Ethiopian rift. *Environmental Challenges*, *6*(August 2021), 100419. https://doi.org/10.1016/j.envc.2021.100419

Gislason, P. O., Benediktsson, J. A., & Sveinsson, J. R. (2006). Random forests for land cover classification. *Pattern Recognition Letters*, *27*(4), 294–300. https://doi.org/10.1016/j.patrec.2005.08.011

Gorelick, N., Hancher, M., Dixon, M., Ilyushchenko, S., Thau, D., & Moore, R. (2017). Google Earth Engine: Planetary-scale geospatial analysis for everyone. *Remote Sensing of Environment*, *202*, 18–27. https://doi.org/10.1016/j.rse.2017.06.031

Herrmann, S. M., Brandt, M., Rasmussen, K., & Fensholt, R. (2020). Accelerating land cover change in West Africa over four decades as population pressure increased. *Communications Earth & Environment*, *1*(1), 1–10. https://doi.org/10.1038/s43247-020-00053-y

Hewitt, R., van Delden, H., & Escobar, F. (2014). Participatory land use modelling, pathways to an integrated approach. *Environmental Modelling and Software*, *52*, 149–165. https://doi.org/10.1016/j.envsoft.2013.10.019

Horning, N. (2004). *Land cover classification methods*.

Jampani, M., Amerasinghe, P., Liedl, R., Locher-Krause, K., & Hülsmann, S. (2020). Multi-functionality and land use dynamics in a peri-urban environment influenced by wastewater irrigation. *Sustainable Cities and Society*, *62*, 62. https://doi.org/10.1016/j.scs.2020.102305

Jean-Claude, B., Rolland, D., & Jean-Christophe, P. (2015). SIMULSEN : logiciel de simulation de gestion d'un barrage à objectifs multiples, au pas de temps journalier : manuel de référence et d'utilisation des versions DOS et Windows XP de décembre 2005 - Mise à jour avril 2015. 103.

Kabanza, A., Dondeyne, S., Tenga, J., Kimaro, D., Poesen, J., Kafiriti, E., & Deckers, J. (2013). More people, more trees in South Eastern Tanzania: Local and global drivers of land-use/cover changes. *African Geographical Review*, *32*(1), 44–58. https://doi.org/10.1080/19376812.2012.746093

Kaku, D. U., Cao, Y., Al-Masnay, Y. A., & Nizeyimana, J. C. (2021). An integrated approach to assess the environmental impacts of large-scale gold mining: The nzema-gold mines in the ellembelle district of Ghana as a case study. *International Journal of Environmental Research and Public Health*, *18*(13), 7044. https://doi.org/10.3390/ijerph18137044

Kulkarni, A. D., & Lowe, B. (2016). Random forest algorithm for land cover classification. *International Journal on Recent and Innovation Trends in Computing and Communication*, *4*(3), 58–63. http://hdl.handle.net/10950/341

Kulkarni, K., & Vijaya, P. (2021). NDBI Based prediction of land use land cover change. *Journal of the Indian Society of Remote Sensing*, *49*(10), 2523–2537. https://doi.org/10.1007/s12524-021-01411-9

Leta, M. K., Demissie, T. A., & Tränckner, J. (2021). Modeling and prediction of land use land cover change

dynamics based on land change modeler (Lcm) in nashe watershed, upper blue nile basin, Ethiopia. *Sustainability (Switzerland)*, *13*(7), 3740. https://doi.org/10.3390/su13073740

Liping, C., Yujun, S., Saeed, S., & Westergaard-Nielsen, A. (2018). Monitoring and predicting land use and land cover changes using remote sensing and GIS techniques—A case study of a hilly area, Jiangle, China. *PLoS ONE*, *13*(7), 1–23. https://doi.org/10.1371/journal.pone.0200493

Lu, D., & Weng, Q. (2007). A survey of image classification methods and techniques for improving classification performance. *International Journal of Remote Sensing*, *28*(5), 823–870. https://doi.org/10.1080/01431160600746456

Macarringue, L. S., Bolfe, É. L., & Pereira, P. R. M. (2022). Developments in land use and land cover classification techniques in remote sensing: A review. *Journal of Geographic Information System*, *14*(1), 1–28. https://doi.org/10.4236/jgis.2022.141001

Ma, L., Liu, Y., Zhang, X., Ye, Y., Yin, G., & Johnson, B. A. (2019). Deep learning in remote sensing applications: A meta-analysis and review. *Isprs Journal of Photogrammetry & Remote Sensing*, *152*, 166–177. November 2018. https://doi.org/10.1016/j.isprsjprs.2019.04.015

Mas, J. F., & Flores, J. J. (2008). The application of artificial neural networks to the analysis of remotely sensed data. *International Journal of Remote Sensing*, *29*(3), 617–663. https://doi.org/10.1080/01431160701352154

Mas, J., Kolb, M., Paegelow, M., Camacho, M. T., Houet, T., Mas, J., Kolb, M., Paegelow, M., Teresa, M., Olmedo, C., & Houet, T. (2014). Inductive pattern-based land use/cover change models : A comparison of four software packages. In *Environmental Modelling & Software* (pp. 94–111). Elsevier. https://doi.org/10.1016/j.envsoft.2013.09.010.hal-01187569HAL

Mekonnen, Y. A., & Manderso, T. M. (2023). Land use/land cover change impact on streamflow using Arc-SWAT model, in case of Fetam watershed, Abbay Basin, Ethiopia. *Applied Water Science*, *13*(5), 1–19. https://doi.org/10.1007/s13201-023-01914-5

Ministere de l'economie et des finances. (2018). *Rapport De L ' Etude Monographique Sur L ' Orpaillage Au*. 48.

Mishra, V., Rai, P., & Mohan, K. (2014). Prediction of land use changes based on land change modeler (LCM) using remote sensing: A case study of Muzaffarpur (Bihar), India. *Journal of the Geographical Institute Jovan Cvijic, SASA*, *64*(1), 111–127. https://doi.org/10.2298/ijgi1401111m

Mishra, V. N., Rai, P. K., Prasad, R., Punia, M., & Nistor, M. M. (2018). Prediction of spatio-temporal land use/land cover dynamics in rapidly developing Varanasi district of Uttar Pradesh, India, using geospatial approach: A comparison of hybrid models. *Applied Geomatics*, *10*(3), 257–276. https://doi.org/10.1007/s12518-018-0223-5

Murgante, B., Misra, S., Rocha, A. M. A., Torre, C., Rocha, J. G., Falcao, M. I., Taniar, D., Apduhan, B. O., & Gervasi, O. (2014). Computational science and its applications.

Nasiri, V., Deljouei, A., Moradi, F., Sadeghi, S. M. M., & Borz, S. A. (2022). Land use and land cover mapping using sentinel-2, Landsat-8 satellite images, and google earth engine: a comparison of two composition methods. *Remote Sensing*, *14*(9), 1977. https://doi.org/10.3390/rs14091977

Ndiaye, K. (2020). *Impact Environnemental Et Sanitaire Dans Le Sud-Est Du Senegal : Exemple Du*.

Noi Phan, T., Kuch, V., & Lehnert, L. W. (2020). Land cover classification using google earth engine and random forest classifier—the role of image composition. *Remote Sensing*, *12*(15), 2411. https://doi.org/10.3390/RS12152411

Noszczyk, T. (2019). A review of approaches to land use changes modeling. *Human and Ecological Risk Assessment*, *25*(6), 1377–1405. https://doi.org/10.1080/10807039.2018.1468994

Nouaceur, Z., Murarescu, O., & Murătoreanu, G. (2020). Rainfall variability and trend analysis of multiannual. *MS Binici and E Acs Water*, *17*(2), 124–144. https://doi.org/10.1515/avutgs-2017-0012

Olofsson, P., Foody, G. M., Herold, M., Stehman, S. V., Woodcock, C. E., & Wulder, M. A. (2014). Remote sensing of environment good practices for estimating area and assessing accuracy of land change. *Remote Sensing of Environment*, *148*, 42–57. https://doi.org/10.1016/j.rse.2014.02.015

Ougahi, J. H., & Mahmood, S. A. (2022). Evaluation of satellite-based and reanalysis precipitation datasets by hydrologic simulation in the Chenab river basin. *Journal of Water and Climate Change*, *13*(3), 1563–1582. https://doi.org/10.2166/wcc.2022.410

Pontius, R. G., & Batchu, K. (2003). Using the relative operating characteristic to quantify certainty in prediction of location of land cover change in India. *Transactions in GIS*, *7*(4), 467–484. https://onlinelibrary.wiley.com/doi/10.1111/1467-9671.00159

Roland, Y. O. (2021). *Dynamique spatio-temporelle des états de surface et influence sur le ruissellement sur un bassin de type sahélien : cas du bassin de Tougou (Nord Burkina Faso)*. https://doi.org/10.13140/RG.2.2.11834.82883

Sambou, M. H. A., Liersch, S., Koch, H., Vissin, E. W., Albergel, J., & Sane, M. L. (2023). Synergies and trade-offs in water resources management in the bafing watershed under climate change synergies and trade-offs in water resources management in the bafing watershed under climate change. *M S Binici and E Acs Water*, *15*(11), 2067. https://doi.org/10.3390/w15112067

Sane, M. L., Sambou, S., Ndione, D. M., & Leye, I. (2020). Moussé Landing SANE et al. Analyse et traitement des séries de débits annuels et mensuels sur le fleuve sénégal. Rev. Ivoir. Sci. Technol, 30, 102–120. http://www.revist.ci

Sane, M. L., Sambou, S., Ndione, D. M., & Leye, I. (2017). *Moussé Landing SANE et al. Analyse et traitement des séries de débits annuels et mensuels sur le fleuve sénégal*. http://www.revist.ci

Sankarrao, L., Ghose, D. K., & Rathinsamy, M. (2021). Predicting land-use change: Intercomparison of different hybrid machine learning models. *Environmental Modelling and Software*, *145*(September), 105207. https://doi.org/10.1016/j.envsoft.2021.105207

Shelestov, A., Lavreniuk, M., Kussul, N., Novikov, A., & Skakun, S. (2017). Exploring Google earth engine platform for big data processing: Classification of multi-temporal satellite imagery for crop mapping. *Frontiers in Earth Science*, *5*(February), 1–10. https://doi.org/10.3389/feart.2017.00017

Silva, L. P. E., Xavier, A. P. C., da Silva, R. M., & Santos, C. A. G. (2020). Modeling land cover change based on an artificial neural network for a semiarid river basin in northeastern Brazil. *Global Ecology and Conservation*, *21*, e00811. https://doi.org/10.1016/j.gecco.2019.e00811

Singh, S. K., Mustak, S., Srivastava, P. K., Szabó, S., & Islam, T. (2015). Predicting spatial and decadal lulc changes through cellular automata Markov chain models using earth observation datasets and geo-information. *Environmental Processes*, *2*(1), 61–78. https://doi.org/10.1007/s40710-015-0062-x

Singh, V. G., Singh, S. K., Kumar, N., & Singh, R. P. (2022). Simulation of land use/land cover change at a basin scale using satellite data and Markov chain model. *Geocarto International*, *37*(26), 11339–11364. https://doi.org/10.1080/10106049.2022.2052976

Solly, B., Dieye, E. H. B., Oumar, S. Y., Jarju, A. M., & Sane, T. (2021). Detection des zones de degradation et de regeneration de la couverture vegetale dans le sud du Senegal a travers l'analyse des tendances de series temporelles modis NDVI et des changements d'occupation des sols a partir d'images landsat. *Revue Francaise de Photogrammetrie et de Teledetection*, *223*, 1–15. https://doi.org/10.52638/rfpt.2021.580

Stehman, S. V. (2014). Estimating area and map accuracy for stratified random sampling when the strata are different from the map classes. *International Journal of Remote Sensing*, *35*(13), 4923–4939. https://doi.org/10.1080/01431161.2014.930207

Szantoi, Z., Jaffrain, G., Gallaun, H., Bielski, C., Ruf, K., Lupi, A., Miletich, P., Giroux, A.-C., Carlan, I., Croi, W., Augu, H., Kowalewski, C., & Brink, A. (2021). Quality assurance and assessment framework for land cover maps validation in the Copernicus hot spot monitoring activity. *European Journal of Remote Sensing*, *54*(1), 538–557. https://doi.org/10.1080/22797254.2021.1978001

Tabutin, D., & Schoumaker, B. (2020). La démographie de l'Afrique subsaharienne au XXIe siècle. *Population*, *75*(2), 169. https://doi.org/10.3917/popu.2002.0169

Tadese, S., Soromessa, T., & Bekele, T. (2021). Analysis of the Current and Future Prediction. *Scientific World Journal*. https://doi.org/10.1155/2021/6685045

Talukdar, S., Singha, P., Mahato, S., Pal, S., Pal, S., Liou, Y.-A., & Rahman, A. (2020). Land-use land-cover classification by machine learning classifiers for satellite observations — a review. *Remote Sensing*, *12*(7), 1135. https://doi.org/10.3390/rs12071135

Thiam, S., Salas, E. A. L., Rholan, N., Delos, A., Almoradie, S., Verleysdonk, S., Adounkpe, J. G., & Komi, K. (2022). Modelling land use and land cover in the transboundary Mono River catchment of togo and Benin using Markov chain and stakeholder ' s perspectives. *Sustainability*, *14*(7), 4160. https://doi.org/10.3390/su14074160

Thiam, S., Villamor, G. B., Faye, L. C., Sène, J. H. B., Diwediga, B., & Kyei-Baffour, N. (2021). Monitoring land use and soil salinity changes in coastal landscape: A case study from Senegal. *Environmental Monitoring and Assessment*, *193*(5). https://doi.org/10.1007/s10661-021-08958-7

Tiné, M., Perez, L., & Molowny-Horas, R. (2019). Hybrid spatiotemporal simulation of future changes in open wetlands: A study of the Abitibi-Témiscamingue region, Québec, Canada. *International Journal of Applied Earth Observation and Geoinformation*, *74*, 302–313. October 2018. https://doi.org/10.1016/j.jag.2018.10.001

Traore, S. S., Dembele, S., Dembele, D., Diakite, N., & Diakite, C. H. (2022). Dynamique de l'occupation du sol et trajectoire du couvert végétal autour de trois sites miniers du Sud Mali entre 1988 et 2019. *Physio-Géo*, *17* (Volume 17), 151–166. https://doi.org/10.4000/physio-geo.14565

Traore, A., Mawenda, J., & Komba, A. (2018). Land-cover change analysis and simulation in conakry (guinea), using hybrid cellular-automata and Markov model. *Urban Science*, *2*(2), 1–16. https://doi.org/10.3390/urbansci2020039

Tsai, Y. H., Stow, D., Chen, H. L., Lewison, R., An, L., & Shi, L. (2018). Mapping vegetation and land use types in Fanjingshan national nature reserve using google earth engine. *Remote Sensing*, *10*(6), 927. https://doi.org/10.3390/rs10060927

UCAD. (2019). *Final report climate vulnerability and water resources variability in West Africa Senegal and Gambia River Basin Cases*. 1–131.

Wahap, N. A., & Shafri, H. Z. M. (2020). Utilization of Google Earth Engine (GEE) for land cover monitoring over Klang Valley, Malaysia. *IOP Conference Series: Earth and Environmental Science*, *540*(1). https://doi.org/10.1088/1755-1315/540/1/012003

Wang, S. W., Munkhnasan, L., & Lee, W. K. (2021). Land use and land cover change detection and prediction in Bhutan's high altitude city of Thimphu, using cellular automata and Markov chain. *Environmental Challenges*, *2*, 100017. November 2020 https://doi.org/10.1016/j.envc.2020.100017 https://doi.org/10.1016/j.envc.2020.100017

Winkler, K., Fuchs, R., Rounsevell, M., & Herold, M. (2019). Global land use changes are four times greater than previously estimated. *Nature Communications*, *2021*(1), 1–10. https://doi.org/10.1038/s41467-021-22702-2

Woodcock, C. E., Allen, R., Anderson, M., Belward, A., Bindschadler, R., Cohen, W., Gao, F., Goward, S. N., Helder, D., Helmer, E., Nemani, R., Oreopoulos, L., Schott, J., Thenkabail, P. S., Vermote, E. F., Vogelmann, J., Wulder, M. A., & Wynne, R. (2008). Free access to Landsat imagery. *Science: Advanced Materials and Devices*, *320*(5879), 1011. https://doi.org/10.1126/science.320.5879.1011a

Yang, L., Driscol, J., Sarigai, S., Wu, Q., Chen, H., & Lippitt, C. D. Google Earth Engine and Artificial Intelligence (AI): A Comprehensive Review. (2022). *Remote Sensing*, *14*(14), 3253. *14*(14). https://doi.org/10.3390/rs14143253

Yang, Y., Yang, D., Wang, X., Zhang, Z., & Nawaz, Z. (2021). Testing accuracy of land cover classification algorithms in the qilian mountains based on gee cloud platform. *Remote Sensing*, *13*(24). https://doi.org/10.3390/rs13245064

Zadbagher, E., Becek, K., & Berberoglu, S. (2018). Modeling land use/land cover change using remote sensing and geographic information systems: Case study of the Seyhan Basin, Turkey. *Environmental Monitoring and Assessment*, *190*(8). https://doi.org/10.1007/s10661-018-6877-y

Zurqani, H. A., Post, C. J., Mikhailova, E. A., Schlautman, M. A., & Sharp, J. L. (2018). Geospatial analysis of land use change in the Savannah River Basin using google earth engine. *International Journal of Applied Earth Observation and Geoinformation*, *69*, 175–185. December 2017. https://doi.org/10.1016/j.jag.2017.12.006